

<https://doi.org/10.1038/s43247-024-01355-1>

Recent increase in the surface mass balance in central East Antarctica is unprecedented for the last 2000 years

Check for updates

Alexey A. Ekaykin¹✉, Arina N. Veres¹ & Yetang Wang²

The Antarctic Ice Sheet's reaction on the continuing global warming is crucial to project the future sea level rise. The increasing air temperature causes both accelerating mass loss on the Antarctica's margins and increased surface mass balance in its interior. Here, we use data from firn cores drilled near Vostok station (central East Antarctica) to analyze the surface mass balance variability over the past 2200 years. We show a 24% increase of snow accumulation rate since early 19 century confirmed by the instrumental data for the last 52 years. The mean surface mass balance value in 1970–2021 ($2.25 \pm 0.064 \text{ g cm}^{-2} \text{ yr}^{-1}$) is very likely unprecedented in the pre-industrial era. The surface mass balance growth is accompanied by the air temperature increase with the sensitivity of $11 \pm 2\%$ per 1°C . These results will help to constrain the potential magnitude of Antarctic snowfall mitigation of future sea level rise.

The final value of the sea level rise by the end of the 21st century will be defined to large extent by the reaction of the Antarctic Ice sheet (AIS) on the ongoing and future climate warming¹. This reaction includes several processes that are sometimes contradictory to each other. On the one hand, in a warmer climate, the ice dynamics accelerates leading to increased mass loss, and the summer melt takes place in larger areas in the marginal parts of the AIS^{2,3}. On the other hand, elevated air temperature results in increased precipitation rate and the surface mass balance (SMB) in the interior of the continent^{4,5}. Thus, understanding the relationship between the SMB in the central parts of the AIS and the air temperature is crucial for projecting the rate of the sea level rise⁶.

In the view of a lack of direct instrumental data on the temporal variability in the SMB⁷, the researchers need to rely upon the estimates produced by regional climate models^{8–12}, although the model results are subject to substantial biases^{12,13}. Another source of information is the SMB time-series extracted from firn and ice core studies¹⁴. The most interesting time scale in this context is the last 2000 years when the climate variability was relatively small and dominated by volcanic and solar activity (and to lesser extent by Milankovitch and greenhouse gas forcing)¹⁵, on which the anthropogenic activity was superimposed since the beginning of the industrial era in the first half of the 19th century.

The available ice-core data on the SMB in central East Antarctica^{14,16–18} suggests that this variable was decreasing since 1000 CE until the beginning of the 19th century. However, this conclusion is based on the data from only 3 locations (Dronning Maud Land

(DML), South Pole (SP) and Dome Fuji), see Fig. 1. Only two records (Dome Fuji and South Pole) cover the whole Common Era, while the third one (DML) only extends back for 740 years. Thus, there is a huge gap in the information on the past temporal SMB variability in central East Antarctica during the past 1–2 millennia.

Since early in the 19th century the trend changed, and the SMB started to increase^{19,20} probably as a reaction to the rising air temperature²¹. This conclusion is based on a compilation of 175 individual firn and ice core records, but their locations are distributed extremely unevenly: again, the majority of the sites are in the DML region, some are in the coastal East Antarctic, and only very few are located in the vast East Antarctic plateau^{19,20}.

Although the SMB trend since 1800 CE is significant, it is to a large extent obscured by a relatively high inter-annual variability (most of which represents noise) typical for SMB time-series¹⁹. Low signal-to-noise ratio in the SMB records combined with a very small number of records covering the past 2000 years prevent us from conclusion that the recent increase in SMB exceeds the limits of the natural variability in the pre-industrial period.

Here, we present a new robust SMB time-series covering the last two millennia obtained in the middle of the East Antarctic Ice Sheet (EAIS) and combined with the instrumental SMB data for the last 52 years, in order to: (1) confirm the increase of the SMB in the past 200 years in central parts of the EAIS; (2) to examine if the present-day SMB values exceed the pre-industrial limits; and (3) to investigate the sensitivity of the SMB to the local air temperature.

¹Arctic and Antarctic Research Institute, Saint Petersburg, Russia. ²Shandong Normal University, Jinan, China. ✉e-mail: ekaykin@aari.ru

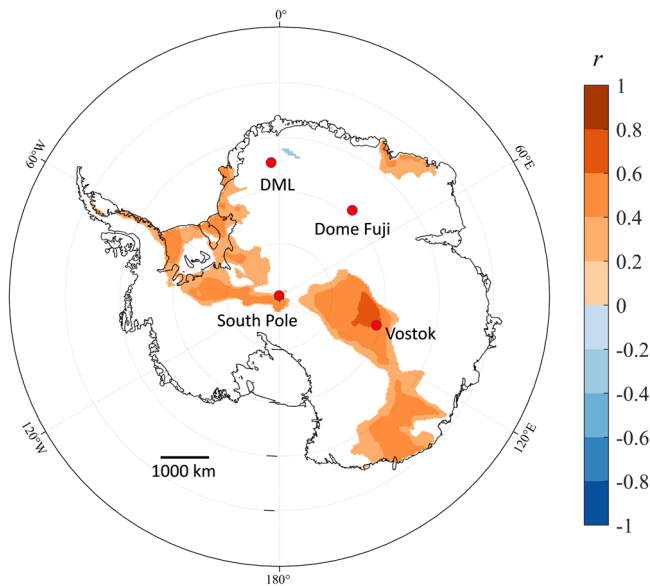


Fig. 1 | The location of the ice core drilling sites mentioned in the paper. DML Dronning Maud Land. The colors denote the spatial variability of the correlation coefficients between detrended time-series of instrumentally measured SMB at Vostok in 1979–2021⁷ and the SMB time-series produced by ERA-5 reanalysis. Only statistically significant correlations ($p < 0.05$) are shown. We used the contour of Antarctica from the Antarctic Digital Database (<https://scar.org/library-data/maps/add-digital-database>). The figure was drawn using the Python programming language.

Results and discussion

Variability of the SMB and air temperature over the past 2000 years

In 2016–2019 three shallow (up to 70.2 m in length) firn cores were drilled near a Russian Antarctic station Vostok (78.465 °S, 106.835 °E, 3490 m above sea level; see Fig. 1 and Supplementary Fig. 1). Electrical conductivity and non-sea-salt sulfate concentration were measured in the cores in order to define the depths of the layers containing the products of well-dated volcanic eruptions (see ‘Firn cores’ in the Methods). This allowed us to establish the depth-age scale for each core, according to which the firn layer at the depth of 70.2 m is dated by 192 BCE²².

The firn density was also measured along all the cores thus allowing us to calculate the mean SMB values for each time interval limited by two adjacent volcanic events (see ‘Surface mass balance’ in the Methods and Supplementary Table 1), see Fig. 2.

The advantage of this time-series lies in the fact that it represents a stack of data from three independent firn cores, which allows us to diminish the amount of noise and to extract reliably the climatic signal in the SMB variability. The distance between the cores (about 2 km) is large enough to assure the absence of ‘noise correlation’ in the adjacent cores and, at the same time, it is small enough to guarantee a common climate variability in all of them⁷.

The new stacked Vostok SMB time-series demonstrates the same character of the millennial variability as was previously observed in the other East Antarctic cores (Fig. 3 and Supplementary Fig. 2): until the 19th century the variability is small with probably a tendency of decreasing SMB values (the rate of the SMB decrease is only 0.5% per millennium). During the period from 168 BCE to 1816 CE the mean SMB is $1.82 \pm 0.05 \text{ g cm}^{-2} \text{ yr}^{-1}$ (hereinafter the uncertainty refers to 1 standard error of mean, SEM).

Since 1816 a clear positive trend is observed, with the mean rate of the SMB increase equal to $0.12 \pm 0.01 \text{ g cm}^{-2} \text{ yr}^{-1}$ per century ($6.8 \pm 0.7\%$ per century). The mean SMB in 1816–2018 is $2.07 \pm 0.05 \text{ g cm}^{-2} \text{ yr}^{-1}$. Similar value ($2.0 \pm 0.07 \text{ g cm}^{-2} \text{ yr}^{-1}$) was independently obtained for the period 1816–1999 as a result of glaciological studies in Vostok snow pits²³ (see ‘Surface mass balance’ section in Methods), Fig. 2 and Supplementary Fig. 3.

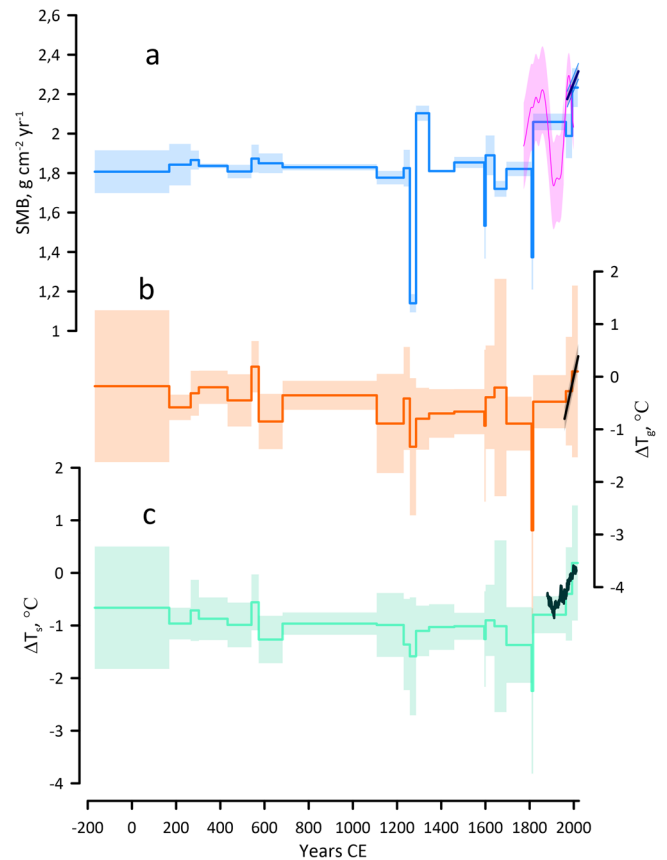


Fig. 2 | Climate variability since 168 BCE extracted from firn cores in the vicinity of Vostok Station (central East Antarctica). a Stack record of surface mass balance (SMB) at Vostok based on the data from 3 firn cores (stepped blue line), from snow pits (magenta) and a linear trend of the SMB in 1970–2021 based on the instrumental observations at Vostok stake farm⁷ (dark blue). b The anomaly (relative to the mean value of the 1988–2018 period) of the local near-surface air temperature (stepped orange line) and a linear trend of the air temperature in 1958–2021 based on instrumental observations at Vostok meteorological station. c Surface air temperature in the moisture source (stepped green line). By dark green line in (c) the anomaly of the Southern Hemisphere sea surface air temperature is shown²⁵. The shading depicts the uncertainty (± 2 standard errors of mean) of the SMB (see ‘Surface mass balance’ in the Methods) and temperature values (see ‘Air temperature reconstruction from stable water isotope data’ in the Methods).

The SMB increase was not monotonic: the growth started at some point in the second half of the 18th century, reached maximum of $2.2 \pm 0.1 \text{ g cm}^{-2} \text{ yr}^{-1}$ in the 1850s, then started to decrease until early in the 20th century when the growth resumed (Supplementary Fig. 3a). A similar variability of SMB was observed at the South Pole: a growth until 1870 followed by a decline until around 1915 (Supplementary Fig. 2). In the other records the start of the present-day SMB increase was detected around 1850 at Dome Fuji and early in the 20th century in the DML region (Fig. 3 and Supplementary Fig. 2).

The recent increase in the surface mass balance is confirmed by the instrumental snow accumulation measurements at the Vostok stake farm⁷: in 1970–2021 the mean SMB was $2.25 \pm 0.064 \text{ g cm}^{-2} \text{ yr}^{-1}$. Interestingly, the instrumental data shows an acceleration of the surface mass balance growth: the mean rate of the SMB increase in 1970–2021 is $0.28 \pm 0.15 \text{ g cm}^{-2} \text{ yr}^{-1}$ per century ($12 \pm 7\%$ per century, see ‘Calculation of the SMB and air temperature trends for the last 200 years’ section in the Methods).

We estimated the probability of a scenario in which similar to present-day SMB values took place in the pre-industrial epoch (see ‘Likelihood of similar to modern SMB and temperature values in the past’ in the Methods). Our calculations show that the likelihood of mean SMB in any 50-year time interval before 1816 equal or higher than $2.25 \pm 0.064 \text{ g cm}^{-2} \text{ yr}^{-1}$ does not

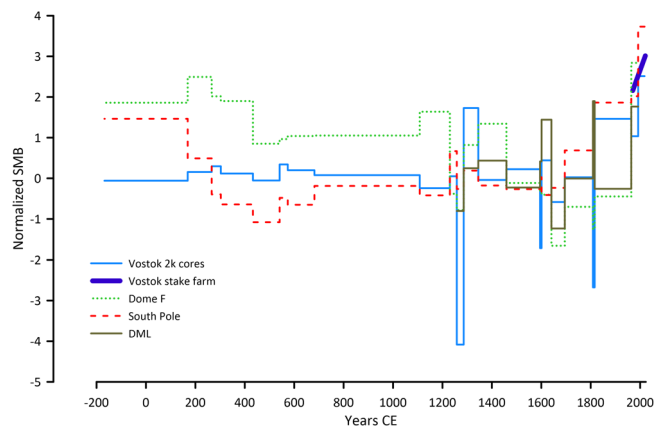


Fig. 3 | Time-series of SMB values over the last 2200 years from 4 East Antarctic sites. Dronning Maud Land (DML) record (brown) is a stack of 3 cores (DML05, DML07 and DML17)³²; Dome Fuji record (dotted green) is a stack of 3 cores (DF1, DF2 and DF1997)¹⁸; South Pole record (dashed red) is from SPICE core¹⁷; Vostok record (blue) is from this work. Also shown by dark blue is a linear trend of the SMB record from Vostok stake farm (1970–2021)⁷. Since the mean SMB values at these sites are different, for the sake of comparison the SMB time-series were normalized respective to their overlapping pre-industrial period (1250–1800). The SMB series from DML, SP and DF are averaged over the same time intervals as in the Vostok record.

exceed 5.7%. This means that the recent increase in Vostok SMB value is unprecedented and is very likely beyond the limits of natural variability for the last 2200 years.

A sharp increase of SMB in the recent decades may not be a unique Vostok phenomenon but likely is a characteristic of a wider area of the Antarctic ice sheet²⁰. To estimate a spatial representativeness of the results obtained at Vostok, we compared the Vostok instrumental SMB time-series in 1979–2021⁷ with the SMB time-series obtained with the use of ERA5 reanalysis and RACMO regional atmospheric climate model (see the methods in Zhai et al.²⁴). The Vostok SMB demonstrates a significant positive correlation with the SMB variability in an extensive (about 2 million km²) part of the East Antarctic plateau (including the vicinity of the South Pole), as well as coastal areas of Weddell sea, Enderby Land and Adelie Land (Fig. 1 and Supplementary Fig. 4). A strong increase of the SMB during the previous 2 decades is observed at the accumulation-stake farm near the South Pole²⁴. Significant trends during the last 200 years are detected in the stack SMB time-series for EAIS and for the whole Antarctic ice sheet, although different EAIS regions demonstrate high variability in the trend values²⁰. In particular, the most recent 50 years (1961–2010) experiences the largest SMB values over the past 300 years as averaged for the whole AIS. Finally, a comparison of the instrumental SMB data²⁴ and the ice core-based SMB time-series at the South Pole¹⁷ leads us to the conclusion that the mean SMB ($9.45 \pm 0.26 \text{ g cm}^{-2} \text{ yr}^{-1}$) over the most recent 50-year (1971–2020) time interval exceeds the mean SMB values over any 50-year interval between 200 BCE and 1800 CE (Fig. 3 and Supplementary Fig. 2) with the probability of 98.6% (see section ‘Likelihood of similar to modern SMB and temperature values in the past’ in the Methods).

The other available East Antarctic core-based SMB time-series confirm that the recent decades are characterized by anomalously high snow accumulation compared to the previous centuries (Fig. 3 and Supplementary Fig. 2): at Dome Fuji the present-day SMB value is the highest since about 350 CE, while in the DML region the recent accumulation rate is the largest in the record (since 1250 CE).

Based on the stable water isotope (δD and $\delta^{18}\text{O}$) measurements in the studied cores (Supplementary Fig. 5) we have also reconstructed the past variability of the local (Vostok) near-surface air temperature T_g (see ‘Air temperature reconstruction from stable water isotope data’ in the Methods and Fig. 2b). The temperature curve shows similar character of centennial variability as that in the SMB time series: a weak cooling trend before 1816

followed by a significant warming afterwards. On average, the local near-surface air temperature at Vostok before 1816 was $0.5 \pm 0.4 \text{ }^\circ\text{C}$ colder than in the present-day (during the last 30 years, 1988–2018). However, the recent increase in the Vostok air temperature cannot be qualified as unprecedented for the past 2000 years because of relatively large error bars in the time-series of T_g due to high spatial variability in δD and $\delta^{18}\text{O}$ values between the adjacent cores.

The technique of the stable water isotope data interpretation allows us simultaneous reconstruction of the temperature in the moisture source T_s in parallel with T_g (see ‘Air temperature reconstruction from stable water isotope data’ in the Methods and Fig. 2c). The T_s values before 1816 were on average $1.0 \pm 0.4 \text{ }^\circ\text{C}$ colder than during the last 30 years (1988–2018), which is in the first approximation corresponds to the sea surface temperature increase in the Southern Hemisphere²⁵.

Interestingly, the stable water isotope data themselves demonstrate only very weak (if any) trend since 1816 (see Supplementary Fig. 5). This happens because the concentration of the heavy water molecules in precipitations depends both on the local air temperature (strictly speaking, on the condensation air temperature) and the temperature in the moisture source. In the case when the both temperatures change in parallel, the isotopic composition in precipitation may not reveal significant shift. It is only when we make use of the second order parameter, ‘deuterium excess’, that we are able to reconstruct the temporal variability of T_g and T_s (see ‘Air temperature reconstruction from stable water isotope data’ in the Methods). This argument could be added to the discussion²¹ of the conundrum of a weak anthropogenic warming trend derived from the core-based stable water isotope records in Antarctica. A recent warming trend obtained in this work is confirmed by the temperature increase detected instrumentally at Vostok station: since 1958 the near-surface air temperature increased by about $1.2 \text{ }^\circ\text{C}$ with a particularly strong rate of warming ($0.6 \text{ }^\circ\text{C}$ per decade) during the last 20 years⁷ (Supplementary Fig. 3b).

Sensitivity of the SMB to the local air temperature

The instrumentally measured SMB at Vostok station in 1970–2021 reveals significant correlation with the mean annual near-surface air temperature with the SMB-temperature sensitivity of $0.24 \pm 0.02 \text{ g cm}^{-2} \text{ yr}^{-1}$ per $1 \text{ }^\circ\text{C}$, or $11 \pm 2\%$ per $1 \text{ }^\circ\text{C}$ ⁷.

According to our new firn core data, since 1816 the median SMB-temperature sensitivity is 12% per $1 \text{ }^\circ\text{C}$ (between 8.8 and 17.2% per $1 \text{ }^\circ\text{C}$), see ‘Calculation of the SMB and air temperature trends for the last 200 years’ in the Methods.

Thus, the Vostok data produces the sensitivity of the SMB to the air temperature that is near the upper end of the range of the published values (between 2 and 10% per $1 \text{ }^\circ\text{C}$ with the average of 5.5% per $1 \text{ }^\circ\text{C}$ ⁴).

The sensitivity of the SMB to temperature is a function of the temperature itself (see ‘Sensitivity of the SMB to air temperature’ in the Methods): the lower is temperature, the stronger is the SMB change per $1 \text{ }^\circ\text{C}$. At Vostok, the mean annual air temperature at the top of the inversion layer (that is used for decades as a proxy of the condensation temperature^{26,27} is $-38.1 \text{ }^\circ\text{C}$ ²⁸, but actual effective condensation temperature could be as low as $-43 \text{ }^\circ\text{C}$ (see ‘Sensitivity of the SMB to air temperature’ in the Methods). With these values, the sensitivity of the SMB to temperature is 9.8–10.2% per $1 \text{ }^\circ\text{C}$ for T_c and 14.6–15.3% per $1 \text{ }^\circ\text{C}$ for T_g , which explains well the results obtained from Vostok firn cores and instrumental data.

The SMB variability at the South Pole in 1983–2020 obtained at the stake farm significantly correlates with the mean annual near-surface air temperature with $r = 0.49 \pm 0.15$ ($p < 0.01$)²⁴. The corresponding SMB-temperature slope is $0.93 \text{ g cm}^{-2} \text{ yr}^{-1}$ per $1 \text{ }^\circ\text{C}$, or $9.5 \pm 2.8\%$ per $1 \text{ }^\circ\text{C}$, i.e., it is similar to the Vostok data.

Conclusion

The new data on the temporal SMB variability during the past 2200 years in central Antarctica (Vostok station) presented here confirms the trends typical for the whole Antarctica: the SMB was stable or slightly decreasing until early in the 19th century followed by a sharp increase in snow

accumulation during the last 200 years. Our data suggests that the present-day Vostok SMB value is very likely unprecedented for the last two millennia. This growth in the SMB seems to be related to the warming near-surface air temperature with the SMB-temperature sensitivity being as large as $11 \pm 2\%$ per 1°C . Similar features (unprecedentedly high SMB values in the recent decades compared to the previous 2 millennia and a strong SMB-temperature gradient) are also observed at the South Pole, which implies that the results of this study are valid for a wide area of the central East Antarctic plateau.

We believe these new findings may be used as an additional constraint for the projections of the Antarctic Ice Sheet's surface mass balance in the course of the continuing global climate change, thus reducing the uncertainty of the AIS's contribution to the sea level rise in the 21st century.

This study stresses the need of developing the network of reliable instrumental SMB observations in central Antarctica, as well as of improvement of the climate models' ability to simulate the SMB and its sensitivity to the air temperature.

Methods

Firn cores

Three shallow firn cores were drilled in the vicinity (in a distance of 1–3 km within the clean sector) of Vostok Station (Supplementary Fig. 1) in 2016–2019 with a use of a light mechanical auger. The cores' lengths were 70, 55, and 65 m. In the glaciological laboratory of Vostok, we first defined the density of the firn by thorough measurements of the cores' volume and mass²⁹.

Then along the core's main axis samples for the stable water isotope analysis were cut (see below) with the resolution of 10 cm.

The electrical conductivity (ECM) was measured continuously along each core to define the position of the layers containing the products of the volcanic eruptions (see below). The rest of one of the cores was shipped to Limnological Institute of Russian Academy of Sciences (Irkutsk, Russia) for chemical analyses. The methods and results are published in Veres et al.²².

Surface mass balance

VK16, VK18 and VK19 firn cores. For the central parts of the East Antarctic plateau the surface mass balance, SMB (a term 'net snow accumulation rate' is used as well as a synonymous) is equal to the difference between bulk snow accumulation (precipitation) and ablation (sublimation)³⁰. The contribution of the meltwater runoff to SMB in the present-day climate of East Antarctic plateau is zero. Based on the firn and ice core data a reconstruction of only the SMB is possible. Usually, it is assumed that the SMB is a reliable proxy of the precipitation in central Antarctica, since the total annual sublimation is relatively small: in the case of Vostok, in the present-day conditions sublimation removes roughly 15–20% of the total annual precipitation³¹.

In the high-accumulation zones (like in central Greenland or in the coastal regions of Antarctica) where annual firn layers can be observed (based on seasonal cycles in the concentration of heavy water isotopes or certain chemical compounds), one can reconstruct annual values of the SMB. In the case of low-accumulation sites like Vostok, only average SMB values between the absolute age markers can be calculated.

Here we use the volcanic age markers identified in all the three cores based on the data on the electrical conductivity and non-marine sulfate concentrations²². In total, 68 volcanic peaks were discovered, of which 22 were attributed to well-dated eruptions. Note that the dates of the firn layers containing the products of the volcanic explosions are 1–2 years younger than the eruptions themselves since it takes time for the volcanic products to reach central Antarctica.

The mean SMB between two adjacent volcanic peaks are calculated based on the available firn density profile²⁹. In particular, in order to define the mean SMB between, e.g., layers of Tambora and Agung, one should divide the relative mass (in g cm^{-2}) of this core section (integrated density profile) by the number of years comprised between these two markers (in this example it equals to $1964 - 1816 = 148$ years).

Two corrections are usually applied to the SMB time series derived from ice core data: (1) for ice advection and (2) for the layer thinning. In this case both of them are negligibly small. With the mean ice velocity of 2 m per year, the oldest firn layers originate about 4 km upstream from the drilling site, where the accumulation rate is the same⁷. The layer thinning is proportional to h/H , where h is the depth of a layer, and H is the total thickness of the glacier, both are in ice equivalent. For the deepest firn layers the correction is about 1%.

The time-series of SMB is shown in Figs. 2, 3 and Supplementary Figs. 2 and 3. The blue shading depicts the uncertainty bars (± 2 standard errors of mean) related to the spatial variability in SMB values. Such spatial variability ('depositional noise') is typical for the snow accumulation in central Antarctica⁷. As an example, the mean SMB between Agung and Pinatubo layers (1964–1992) is $1.89 \text{ g cm}^{-2} \text{ yr}^{-1}$ in one core, $1.99 \text{ g cm}^{-2} \text{ yr}^{-1}$ in the second one and $2.085 \text{ g cm}^{-2} \text{ yr}^{-1}$ in the third core. The mean of the three cores is $1.99 \text{ g cm}^{-2} \text{ yr}^{-1}$ with the standard deviation (STD) of $0.10 \text{ g cm}^{-2} \text{ yr}^{-1}$ and the standard error of mean (SEM, defined as STD divided by the square root of the number of observations) is $0.06 \text{ g cm}^{-2} \text{ yr}^{-1}$. The mean SMB values between the adjacent volcanic markers with the corresponding uncertainty values are listed in Supplementary Table 1.

Note that this 'depositional noise' is typical not only for the SMB time-series, but also for the other cores' properties including the stable water isotopic content (see the next section).

Stack SMB data from snow pits. The SMB values were reconstructed as a result of glaciological works in several snow pits excavated in the vicinity of Vostok station²³. As a basis for reconstruction, the stratigraphic description of the snow thickness was used assuming that on average each snow layer represents 1 year. Because of annual layer hiatus, this method underestimates the number of years comprised in a snow thickness, so absolute age markers are needed to correct the initial dating. As such markers, high beta-activity layers of 1955 and 1965, as well as high acidity volcanic layers of 1816 CE (Tambora) and 1809 CE (unknown event) were used. The annual layer thicknesses (in cm snow equiv.) were multiplied by their densities in order to obtain the SMB values in water equivalents. The SMB time-series from individual pits were used to construct the stacked SMB record, which comprises data from 3 pits in 1773–1949 and 8 pits in 1950–1999. In this study, we smoothed this stack record with a 50-year filter to get rid of high-frequency stratigraphic noise.

SMB data from other locations. In this work, we use data from other East Antarctic sites where sufficiently long SMB time-series are available: Dronning Maud Land (DML), Dome Fuji (DF) and South Pole (SP) (Fig. 1).

The DML SMB record^{14,32} represents a stack of three individual cores: DML07, DML05 and DML17 located not far one from another in an inland part of the Dronning Maud Land region (latitude between 75.0 and 75.58°S and longitude between 3.4°W and 6.5°E). The stacked record was smoothed with a 50-year filter.

The DF record¹⁸ is a stack of three individual cores: DF1, DF2, and DF1997 located in a close vicinity from each other near the Dome Fuji station (77.316°S and 39.701°E).

The SP record is reconstructed based on the geochemical data from the SPICE ice core drilled not far from the Amundsen Scott station¹⁷. The original time-series was smoothed with a 50-year filter. We also use the instrumental SMB data from the SP stake farm in 1983–2020²⁴.

The mean SMB values differ by 1 order of magnitude in different locations, so for the sake of comparison we normalized the records respective to their common pre-industrial period (1250–1800). The data is shown in Fig. 3 and Supplementary Fig. 2.

Air temperature reconstruction from stable water isotope data

The measurements of the concentration of heavy water isotopes ($\delta^{18}\text{O}$ and δD) were performed in Climate and Environmental Research Laboratory of

Arctic and Antarctic Research Institute with the use of Picarro L2130-*i* and L2140-*i* analyzers. The analytical precision was estimated by re-measurement of 10% of randomly chosen samples and was equal to 0.05 and 0.5‰ for δ¹⁸O and δD, correspondingly.

As a result of the measurements we obtained the vertical profiles of the δ¹⁸O, δD and deuterium excess ($dxs = \delta D - 8 \cdot \delta^{18}O$) for each core with the resolution of 10 cm. These vertical profiles were then transformed into the time-series of the same parameters using the depth-age scale developed in Veres et al.²².

Then based on these time-series we calculated the mean isotopic values for the same time intervals for which the SMB data are available (Supplementary Fig. 5).

Note a rather wide uncertainty envelopes (±2 SEM) around the mean values of δ¹⁸O and dxs in Supplementary Fig. 5. This uncertainty is not related to the instrumental error of the isotopic measurements (which is 1–2 orders of magnitude smaller), but with the spatial variability of the isotopic values between different cores due to a high fraction of the ‘depositional noise’ in the total variance of the isotopic values in individual cores.

It is argued that a logarithmic formulation of deuterium excess rather than classical linear formulation is preferable when studying the past temperature based on the ice core stable water isotopic data²⁷. However, when the climate variability is relatively small (as for the last 2000 years in central Antarctica) and the range of isotopic values is small as well, then the linear dxs produces the same result as the logarithmic one²⁷. Thus, in this study, we use the linear dxs for simplicity.

To define the past local air temperature from the isotopic data we used a simple isotope model tuned so that to reproduce the present-day isotopic composition of Vostok snow³³. Such models are designed to solve direct task (to calculate the isotopic composition of snow for given values of moisture source and condensation temperatures), while solving an inverse task is a challenge. To reconstruct the temperature in moisture source T_s and the condensation temperature T_c we applied a Monte Carlo approach: the model randomly chose T_s and T_c from a wide range of possible values and calculated the isotopic composition of Vostok snow. If the obtained δD and dxs values were equal (within uncertainty) to the real ones, such a solution was remembered, otherwise rejected. The calculations were repeated thousands of times before at least 100 correct solutions were found. This procedure was performed for each time interval of our isotopic time-series from the firn cores. This approach has two advantages: (1) it does not assume a linear relationship between isotopic composition and temperature and (2) it allows us to automatically estimate the uncertainty of the temperature reconstruction.

We also attempted to apply a simplified approach developed by Cuffey and Vimeux^{34,35}. The method is based on the assumption that both isotopic content (either δ¹⁸O or δD) and dxs linearly depend on the local condensation temperature and the sea surface temperature in the moisture source:

$$\Delta\delta D = a\Delta T_c - b\Delta T_s \tag{1}$$

and

$$\Delta dxs = -c\Delta T_c + d\Delta T_s \tag{2}$$

where Δ denotes the deviation from the present-day values (i.e., from the mean over the 1988–2018 period).

Another parameter affecting δD and dxs is the relative humidity in the moisture source, but it is considered to be a function of T_s . It is not possible to reconstruct the relative humidity independently from T_s unless a third independent isotopic characteristic (‘17O-excess’) is involved³⁶.

When reconstructing the temperature during cold glacial epochs, the change in the sea water isotopic composition must be taken into account, as well, but for the last 2000 years this factor is negligible³⁷.

From this system of equations, it is easy to derive T_c and T_s as a function of δD and dxs :

$$\Delta T_c = \frac{d\Delta\delta D + b\Delta dxs}{ad - cb} \tag{3}$$

and

$$\Delta T_s = \frac{a\Delta dxs + c\Delta\delta D}{ad - cb} \tag{4}$$

The values of coefficients a , b , c and d are taken from a simple isotope model³³ tuned so as to reproduce the present-day Vostok snow isotopic composition: $a = 10.25 \pm 0.5\text{‰} \text{ }^\circ\text{C}^{-1}$, $b = 3.2 \pm 0.4\text{‰} \text{ }^\circ\text{C}^{-1}$, $c = 1.55 \pm 0.17\text{‰} \text{ }^\circ\text{C}^{-1}$ and $d = 1.71 \pm 0.05\text{‰} \text{ }^\circ\text{C}^{-1}$. The present-day values (the means for 1988-2018 period) of δ¹⁸O, δD and dxs are −57.16‰, −440.97‰ and 16.3‰, correspondingly.

The both methods provide very close reconstructions of the moisture source and condensation temperatures, which justifies the validity of the second approach (based on the Eqs. 3 and 4) for the purpose of this study. We should note, that this simplified method is not applicable to reconstruct larger temperature shifts because of a non-linear character of the isotope-temperature relationship²⁷.

The time-series of the Δ T_c is then reduced to the time-series of the near surface air temperature Δ T_g applying a scaling factor of 0.67: Δ $T_g = \Delta T_c / 0.67$ ²⁷.

One can note that the uncertainty of the temperature reconstructions (Fig. 2b, c) are relatively larger than the uncertainty of the isotopic time-series (Supplementary Fig. 5), which is explained by the summation of the uncertainties of δD and dxs .

We performed another series of tests with different values of the a - d coefficients in order to investigate the sensitivity of the results to the uncertainty of the isotope-temperature gradients. These tests showed that about 90% of the uncertainty of our temperature reconstruction is related to the uncertainty of the isotopic values, while only about 10% are attributed to the uncertainty in the isotope-temperature sensitivities.

Another approach to interpret the heavy stable water isotope concentration in Antarctic cores is to incorporate isotopic fractionation into atmospheric general circulation models³⁸. However, it will not necessarily improve the accuracy of the temperature reconstruction. Firstly, the GCMs still demonstrate substantial biases in the SMB and air temperature values in central Antarctica. Secondly, the temporal isotope-temperature gradients produced by simple models and by GCMs are equal within 20-30% of uncertainty. In general, despite the fact that simple isotope models do not reproduce the complexity of the processes of the atmospheric moisture fractionation, they are successfully used for paleotemperature reconstructions based on ice core isotope data²⁷.

Calculation of the SMB and air temperature trends for the last 200 years

To calculate the SMB trend during the last 200 years of the core-based time-series (Fig. 2) we used the SMB data from 5 intervals (Supplementary Table 1): 1695–1809, 1809–1816, 1816–1964, 1964–1992, and 1992–2018. The interval 1695-1809 is the one when the SMB growth began (Supplementary Fig. 3), so it needs to be taken into account in order to cover the whole SMB range from pre-industrial to the present-day. For each interval we constructed a normal distribution of the SMB values using the mean and the uncertainty as listed in Supplementary Table 1. Then for each interval a SMB value is randomly chosen from the corresponding distribution, and these values are used to construct a step-like SMB time-series for 1695-2018 with annual resolution, and this time series is used to calculate a linear trend of SMB. Then this procedure is repeated 10⁵ times in order to collect a reliable statistic of possible range of the SMB trends taking into account the SMB uncertainty for each time interval.

The same Monte Carlo approach is applied to calculate temperature trends with the use of the Eqs. 3 and 4 (see the previous section) and the δD and dxs values with their uncertainties (Supplementary Fig. 5). The SMB-temperature sensitivity values are calculated for each pair of SMB and temperature trends, so as a result we obtain an array of 10^5 individual sensitivity values which allows to describe the distribution of this parameter. A small amount of temperature trend calculations occasionally produces values close to 0, which gives a very large values of SMB-temperature sensitivity. Due to this, the distribution of the sensitivities is not normal, and the percentiles are preferable to describe it instead of the mean and standard deviation. In particular, the median of the SMB-temperature sensitivity is equal to $0.22 \text{ g cm}^{-2} \text{ yr}^{-1} \text{ }^\circ\text{C}^{-1}$ ($12.5\% \text{ }^\circ\text{C}^{-1}$) and the 5th, 17th, 83th, and 95th percentiles are, correspondingly, 0.11, 0.16, 0.31, and $0.40 \text{ g cm}^{-2} \text{ yr}^{-1} \text{ }^\circ\text{C}^{-1}$ (6.0, 8.8, 17.2, and $22.4\% \text{ }^\circ\text{C}^{-1}$).

Likelihood of similar to modern SMB and temperature values in the past

According to the instrumental measurements⁷, the mean SMB value at Vostok over the past 52 years (1970–2021) is $2.25 \pm 0.064 \text{ g cm}^{-2} \text{ yr}^{-1}$ (± 1 SEM). This value is considerably higher than those observed before 1816: the maximum SMB in the pre-industrial epoch ($2.1 \pm 0.019 \text{ g cm}^{-2} \text{ yr}^{-1}$) was observed in 1286–1345. However, a strong decadal SMB variability, similar to that observed in the snow pit SMB time-series in 1773–1999 (Fig. 2 and Supplementary Fig. 3), exists within any of the time intervals of our firn core SMB record shown in Fig. 2.

What is the probability that mean SMB during any of a 50-year time interval before 1816 was larger than the mean over the last 50 years? To answer this question we, first of all, need to estimate a temporal climatic variability of the 50-year mean SMB values ($\sigma_{50\text{yrs}}$).

In our stack SMB record (Fig. 2) we have 3 periods with the lengths close to 50 years: 1286–1345 (59 years), 1601–1641 (40 years) and 1641–1695 (54 years). The standard deviation (STD) of the mean SMB values in these 3 intervals is $0.19 \text{ g cm}^{-2} \text{ yr}^{-1}$, which can be used as a first-order approximation of $\sigma_{50\text{yrs}}$.

Let us verify if this value corresponds to an expected inverse relationship between the STD of a mean SMB value and the length of a time interval for which this mean SMB is defined. For this we grouped the mean SMB values into 4 clusters according to the lengths of their intervals: (1) 28–37 years (4 values, average length is 32 years, STD of the mean SMB values is $0.36 \text{ g cm}^{-2} \text{ yr}^{-1}$), (2) 40–59 years (3 values, average length is 51 years, STD is $0.19 \text{ g cm}^{-2} \text{ yr}^{-1}$), (3) 97–136 years (8 values, average length is 120 years, STD is $0.026 \text{ g cm}^{-2} \text{ yr}^{-1}$), and (4) 337–426 years (2 values, average length is 382 years, STD is 0.016). Note that we used only SMB data prior to 1816 since we are interested in studying the pre-industrial climate variability. As expected, the variability of the mean snow accumulation rates decreases when the period of observation increases (Supplementary Fig. 6), and the approximation curve closely describes the data points with R^2 of 0.9.

However, the $\sigma_{50\text{yrs}}$ value is estimated based on only 3 datapoints, so one can argue that this estimation is biased relative to the true value. Thus, we independently calculated $\sigma_{50\text{yrs}}$ using the stacked Vostok SMB time-series for 1773–1999 (Supplementary Fig. 3). For this SMB dataset the climate variability of the 50-year mean SMB values equals to $0.18 \text{ g cm}^{-2} \text{ yr}^{-1}$. We believe that in 1773–1999 the climate SMB variability could be stronger than before 1773, since the last 200 years was a period of a strong SMB growth.

Thus, we use the value of $0.19 \text{ g cm}^{-2} \text{ yr}^{-1}$ as a reliable (probably, slightly overestimated) approximation of $\sigma_{50\text{yrs}}$.

Then we also need to take into account the uncertainty of the mean SMB values of the time intervals between the volcanic age markers (Supplementary Table 1) related to the spatial variability of SMB between the cores ('depositional noise'), σ_{DN} . For this we first constructed the relationship between the standard error of mean (SEM) SMB value for a given time interval and the length of this interval (Supplementary Fig. 7).

As expected, σ_{DN} decreases with the increase of the length of the intervals. However, when we define σ_{DN} based on only 3 cores, its value may

be underestimated because all 3 values may occasionally be close to each other. To avoid this, we adopted the following rule: we compare σ_{DN} value for a given interval as defined from the data (Supplementary Table 1) and as calculated from the approximation equation (Supplementary Fig. 7) and choose the larger one.

The final estimate of the climatic variability of a mean 50-years SMB value for given time interval is thus:

$$\sigma_{\text{total}} = (\sigma_{50\text{yrs}}^2 + \sigma_{\text{DN}}^2)^{1/2} \quad (5)$$

Then for each time interval in our firn core SMB record (Fig. 2) longer than 100 years we calculated the normal distribution with the mean equal to the mean SMB of this interval (Supplementary Table 1) and the standard deviation equal to σ_{total} . We randomly sampled values of this distribution and compared them with randomly chosen values from the distribution of the mean SMB values for the last 50 years⁷ (1970–2021, the mean SMB equals to $2.25 \text{ g cm}^{-2} \text{ yr}^{-1}$ and standard deviation equals to $0.064 \text{ g cm}^{-2} \text{ yr}^{-1}$). We repeated this procedure 10^5 times for each interval and calculated the number of cases when a SMB value from the 1970–2021 distribution was smaller than a SMB value from the distribution of a corresponding interval.

These calculations show that the likelihood of any 50-year time interval before 1816 having SMB larger than in 1970–2021 does not exceed 2.5% (for the interval 1459–1595 CE).

Another procedure was applied to the 1286–1345 CE interval (mean SMB = $2.1 \pm 0.019 \text{ g cm}^{-2} \text{ yr}^{-1}$). The length of this interval is 59 years. Let's assume that this interval consists of two intervals: 9 years with lower SMB and 50 years with higher SMB, so that

$$\text{SMB}_{59\text{yrs}} = (\text{SMB}_{9\text{yrs}} \times 9 + \text{SMB}_{50\text{yrs}} \times 50) / 59 \quad (6)$$

Thus, the mean SMB of the 50-year interval is:

$$\text{SMB}_{50\text{yrs}} = (\text{SMB}_{59\text{yrs}} \times 59 - \text{SMB}_{9\text{yrs}} \times 9) / 50 \quad (7)$$

We constructed normal distributions for $\text{SMB}_{59\text{yrs}}$ (mean = 2.1 and $\text{STD} = 0.019 \text{ g cm}^{-2} \text{ yr}^{-1}$) and for $\text{SMB}_{9\text{yrs}}$ (mean = 2.1 and $\text{STD} = \sigma_{\text{total}}$, where $\sigma_{\text{total}} = (\sigma_{50\text{yrs}}^2 + \sigma_{\text{DN}}^2)^{1/2}$; $\sigma_{9\text{yrs}} = 0.34 \text{ g cm}^{-2} \text{ yr}^{-1}$, as estimated from the stack snow pit SMB dataset for 1773–1999; and $\sigma_{\text{DN}} = 0.019 \text{ g cm}^{-2} \text{ yr}^{-1}$). We randomly sampled $\text{SMB}_{59\text{yrs}}$ and $\text{SMB}_{9\text{yrs}}$ distributions 10^5 times in order to calculate $\text{SMB}_{50\text{yrs}}$ according to Eq. (7), and then $\text{SMB}_{50\text{yrs}}$ was compared with randomly chosen values from the 1970–2021 SMB distribution. These exercises lead to the conclusion that with probability of 5.7% the SMB value during the 1286–1345 CE interval could exceed the SMB during the most recent 50 years.

Similar calculations were performed for the South Pole SMB data obtained as a result of instrumental observations at the stake farm (1983–2020)²⁴ and from the ice core (200 BCE to 2014 CE)¹⁷. First, we constructed the SMB time-series for 1970–2020 by combining the stake farm data with the most recent part of the ice core data and calculated the mean and the SEM for this interval. Then we calculated the mean and SEM values for the 50-year intervals for the ice core data from the present-day to 200 BCE. Then we used the same procedure as described above for Vostok. The mean SMB during the most recent 50-year interval is $9.45 \pm 0.26 \text{ g cm}^{-2} \text{ yr}^{-1}$. The highest pre-industrial SMB value ($8.58 \pm 0.29 \text{ g cm}^{-2} \text{ yr}^{-1}$) was observed in 59–9 BCE. The likelihood that the first is less than the second is 1.4%.

As for the air temperature at Vostok, the present-day values are higher than in the pre-1816 period except for 541–574 CE (Fig. 2). However, due to large uncertainties of the temperature reconstruction, it is not possible to conclude that the recent temperature increase is unprecedented for the pre-industrial period.

Sensitivity of the SMB to air temperature

It is assumed that the sensitivity of the Antarctic surface mass balance (SMB) to the air temperature in central Antarctica is proportional to the Clausius-

Clapeyron relationship, which describes the saturation water vapor pressure e_s as a function of temperature T ²⁹:

$$\frac{dln e_s}{dT} = \frac{L}{R_v T^2} \equiv \alpha(T) \quad (8)$$

where L is the latent heat of vaporization ($2.5 \times 10^6 \text{ J kg}^{-1}$), R_v is the specific gas constant for water vapor ($461 \text{ J K}^{-1} \text{ kg}^{-1}$) and T is in K. Here T is the effective condensation temperature T_c , which in the case of the central Antarctic is usually approximated by the air temperature at the top of the inversion layer T_{inv} ²⁶. At Vostok, the mean value of T_{inv} for the period of 1963–1991 (when the balloon-sounding data is available) is -38.1°C ($=235.05 \text{ K}$)²⁸, and the corresponding SMB-temperature sensitivity α is 9.8% per 1°C . However, it is argued that so-called ‘diamond dust’ (a form of precipitation typical for central Antarctica) is formed not on the top of the inversion, but rather in the whole inversion layer, as soon as air is cooling during its descent towards the surface. In this case, the effective condensation temperature would be much colder. For Vostok, T_c was estimated to be about -43°C ^{28,33} (about 230 K), and the corresponding sensitivity is 10.2% per 1°C .

Then, if we want to calculate the sensitivity of the SMB to the near-surface air temperature, we need to consider different amplitude of temperature variability in the inversion layer and in the near-surface layer. It is assumed that the slope between temporal variability of T_g and T_c is 0.67 ^{26,27}, i.e., the amplitude of condensation temperature is 0.67 times that of the near-surface temperature. Applying this coefficient, we obtain the slope between the SMB and T_g equal to about 15% per 1°C for the condensation temperature of -43°C .

Thus, a relatively strong SMB-temperature sensitivity obtained for Vostok can be easily explained by a very cold temperatures typical for this region.

When considering the relationship between the SMB and temperature, one should remember that the Clausius–Clapeyron equation describes the sensitivity of precipitation to temperature, rather than of the SMB. As mentioned above (see ‘Surface mass balance’ in the Methods) the SMB in central Antarctica is the difference of precipitation and sublimation. The sublimation rate is also related to temperature³¹: the warmer is air, the stronger is sublimation. Thus, the total sensitivity of the SMB to temperature may be slightly weaker than that predicted by the Clausius–Clapeyron relationship.

Data availability

The data presented in this manuscript is deposited to Zenodo storage (<https://zenodo.org/records/10719025>).

Received: 15 August 2023; Accepted: 28 March 2024;

Published online: 13 April 2024

References

- Stokes, C. R. et al. Response of the East Antarctic Ice Sheet to past and future climate change. *Nature* **608**, 275–287 (2022).
- Kittel, C. et al. Diverging future surface mass balance between the Antarctic ice shelves and grounded ice sheet. *Cryosphere* **15**, 1215–1236 (2021).
- Park, J. Y. et al. Future sea-level projections with a coupled atmosphere–ocean–ice–sheet model. *Nat. Commun.* **14**, 1–11 (2023).
- Nicola, L., Notz, D. & Winkelmann, R. Revisiting temperature sensitivity: how does Antarctic precipitation change with temperature? *Cryosphere* **17**, 2563–2583 (2023).
- Siahaan, A. et al. The Antarctic contribution to 21st-century sea-level rise predicted by the UK Earth System Model with an interactive ice sheet. *Cryosphere* **16**, 4053–4086 (2022).
- Slater, T., Hogg, A. E. & Mottram, R. Ice-sheet losses track high-end sea-level rise projections. *Nat. Clim. Change* **10**, 877–881 (2020).
- Ekaykin, A. A., Lipenkov V.Y. & Tebenkova, N. A. Fifty years of instrumental surface mass balance observations at Vostok Station, central Antarctica. *J. Glaciol.* 1–13 <https://doi.org/10.1017/jog.2023.53> (2023).
- Agosta, C. et al. Estimation of the Antarctic surface mass balance using the regional climate model MAR (1979–2015) and identification of dominant processes. *Cryosphere* **13**, 281–296 (2019).
- Dunmire, D., Lenaerts, J. T. M., Datta, R. T. & Gorte, T. Antarctic surface climate and surface mass balance in the Community Earth System Model version 2 during the satellite era and into the future (1979–2100). *Cryosphere* **16**, 4163–4184 (2022).
- Mottram, R. et al. What is the surface mass balance of Antarctica? An intercomparison of regional climate model estimates. *Cryosphere* **15**, 3751–3784 (2021).
- van Wessem, J. M. et al. Modelling the climate and surface mass balance of polar ice sheets using RACMO2 – Part 2: Antarctica (1979–2016). *Cryosphere* **12**, 1479–1498 (2018).
- Wang, Y. et al. A comparison of Antarctic ice sheet surface mass balance from atmospheric climate models and in situ observations. *J. Clim.* **29**, 5317–5337 (2016).
- Richter, A. et al. Surface mass balance models vs. stake observations: a comparison in the lake Vostok region, central East Antarctica. *Front. Earth Sci.* **9**, 1–14 (2021).
- Thomas, E. R. et al. Regional Antarctic snow accumulation over the past 1000 years. *Clim. Past* **13**, 1491–1513 (2017).
- Cartapanis, O., Jonkers, L., Moffa-Sanchez, P., Jaccard, S. L., & de Vernal, A. Complex spatio-temporal structure of the Holocene Thermal Maximum. *Nat. Commun.* **13**, 1–11 (2022).
- Mosley-Thompson, E., Paskevitch, J. F., Gow, A. J. & Thompson, L. G. Late 20th century increase in South Pole accumulation. *J. Geophys. Res.* **104**, 3877–3886 (1999).
- Winski, D. A. et al. The SP19 chronology for the South Pole Ice Core – Part 1: volcanic matching and annual layer counting. *Clim. Past* **15**, 1793–1808 (2019).
- Oyabu, I. et al. Temporal variations of surface mass balance over the last 5000 years around Dome Fuji, Dronning Maud Land, East Antarctica. *Clim. Past* **19**, 293–321 (2023).
- Medley, B. & Thomas, E. R. Increased snowfall over the Antarctic Ice Sheet mitigated twentieth-century sea-level rise. *Nat. Clim. Change* **9**, 34–39 (2019).
- Wang, Y. & Xiao, C. An increase in the Antarctic surface mass balance during the past three centuries, dampening global sea level rise. *J. Clim.* **36**, 8127–8138 (2023).
- Casado, M., Hebert, R., Faranda, D. & Landais, A. The quandary of detecting the signature of climate change in Antarctica. *Nat. Clim. Change* **13**, 1082–1088 (2023).
- Veres, A. N. et al. A record of volcanic eruptions over the past 2,200 years from Vostok firn cores, central East Antarctica. *Front. Earth Sci.* **11**, 1075739 (2023).
- Ekaykin, A. A. et al. The changes in isotope composition and accumulation of snow at Vostok Station over the past 200 years. *Ann. Glaciol.* **39**, 569–575 (2004).
- Zhai, Z., Wang, Y., Lazzara, M. A., Keller, L. M. & Wu, Q. Snow accumulation variability at the South Pole from 1983 to 2020, associated with Central Tropical Pacific forcing. *J. Geophys. Res. Atmos.* **128**, 1–14 (2023).
- NOAA extended reconstruction Sea Surface Temperatures v.4: <https://climatedataguide.ucar.edu/climate-data/sst-data-noaa-extended-reconstruction-ssts-version-4>.
- Jouzel, J. & Merlivat, L. Deuterium and oxygen 18 in precipitation: Modeling of the isotopic effects during snow formation. *J. Geophys. Res. Atmos.* **89**, 11749–11757 (1984).
- Markle, B. R. & Steig, E. J. Improving temperature reconstructions from ice-core water-isotope records. *Clim. Past* **18**, 1321–1368 (2022).

28. Ekaykin, A. Meteorological regime of central Antarctica and its role in the formation of isotope composition of snow thickness. *Thesis for the Degree of Doctor of University Grenoble 1*, 122 (2003).
29. Ekaykin, A. A. et al. Vertical profile of snow-firn density in the vicinity of Vostok station, Central Antarctica. *Ice Snow* **62**, 504–511 (2022).
30. Eisen, O. et al. Ground-based measurements of spatial and temporal variability of snow accumulation in East Antarctica. *Rev. Geophys.* **46**, RG2001 (2008).
31. Ekaykin, A. A., Zarovchatskiy, V. A. & Lipenkov, V. Y. Measurements of snow sublimation rate at Vostok station (Antarctica). *Arctic Antarct. Res.* **4**, 20–25 (2015).
32. Oerter, H. et al. Accumulation rates in Dronning Maud Land, Antarctica, as revealed by dielectric-profiling measurements of shallow firn cores. *Ann. Glaciol.* **30**, 27–34 (2000).
33. Salamatin, A. N., Ekaykin, A. A. & Lipenkov, V. Y. Modelling isotopic composition in precipitation in Central Antarctica. *Ice Snow* **97**, 24–34 (2004).
34. Cuffey, K. M. & Vimeux, F. Covariation of carbon dioxide and temperature from the Vostok ice core after deuterium-excess correction. *Nature* **412**, 523–527 (2001).
35. Vimeux, F., Cuffey, K. M. & Jouzel, J. New insights into Southern Hemisphere temperature changes from Vostok ice cores using deuterium excess correction. *Earth Planet. Sci. Lett.* **203**, 829–843 (2002).
36. Veres, A. N. et al. Climatic variability in the era of MIS11 (370–440 ka BP) according to isotope composition (δD , $\delta^{18}O$, $\delta^{17}O$) of ice from the Vostok station cores. *Ice Snow* **58**, 149–158 (2018).
37. Jones, R. S. et al. Stability of the Antarctic Ice Sheet during the pre-industrial Holocene. *Nat. Rev.* **3**, 500–515 (2022).
38. Goursaud, S., Masson-Delmotte, V., Favier, V., Orsi, A. & Werner, M. Water stable isotope spatio-temporal variability in Antarctica in 1960–2013: observations and simulations from the ECHAM5-wiso atmospheric general circulation model. *Clim. Past* **14**, 923–946 (2018).
39. Held, I. M. & Soden, B. J. Robust responses of the hydrological cycle to global warming. *J. Clim.* **19**, 5686–5699 (2006).

Acknowledgements

We thank Editors Dr. Rachael Rhodes, Dr. Alienor Lavergne and Dr. Kathleen Williamson, as well as Dr. Marie Cavitte and two anonymous reviewers for the positive criticism and the valuable suggestions on how to improve the manuscript. This work has been financed by Russian Science Foundation grant 21-17-00246.

Author contributions

A.E. and A.V. participated in the field works (firn drilling and core processing) and laboratory measurements of the stable water isotope concentrations, and prepared the manuscript, Y.W. performed the SMB modeling with the use of ERA5 and RACMO.

Competing interests

The authors declare no competing interests.

Additional information

Supplementary information The online version contains supplementary material available at <https://doi.org/10.1038/s43247-024-01355-1>.

Correspondence and requests for materials should be addressed to Alexey A. Ekaykin.

Peer review information *Communications Earth & Environment* thanks Marie Cavitte and the other, anonymous, reviewer(s) for their contribution to the peer review of this work. Primary Handling Editors: Rachael Rhodes and Alienor Lavergne. A peer review file is available

Reprints and permissions information is available at <http://www.nature.com/reprints>

Publisher's note Springer Nature remains neutral with regard to jurisdictional claims in published maps and institutional affiliations.

Open Access This article is licensed under a Creative Commons Attribution 4.0 International License, which permits use, sharing, adaptation, distribution and reproduction in any medium or format, as long as you give appropriate credit to the original author(s) and the source, provide a link to the Creative Commons licence, and indicate if changes were made. The images or other third party material in this article are included in the article's Creative Commons licence, unless indicated otherwise in a credit line to the material. If material is not included in the article's Creative Commons licence and your intended use is not permitted by statutory regulation or exceeds the permitted use, you will need to obtain permission directly from the copyright holder. To view a copy of this licence, visit <http://creativecommons.org/licenses/by/4.0/>.

© The Author(s) 2024